



OPEN Multi-omics study reveals differential expression and phosphorylation of autophagy-related proteins in autism spectrum disorder

Eden Deri¹, Shashank Kumar Ojha¹, Maryam Kartawy¹, Igor Khaliulin¹ & Haitham Amal^{1,2,3}✉

Our multi-omics study investigated the molecular mechanisms underlying autism spectrum disorder (ASD) using *Shank3*^{Δ4–22} and *Cntnap2*^{−/−} mouse models. Through global- and phospho- proteomics of the mouse cortex, we focused on shared molecular changes and found that autophagy was particularly affected in both models. Global proteomics identified a small number of differentially expressed proteins that significantly impact postsynaptic components and synaptic function, including key pathways such as mTOR signaling. Phosphoproteomics revealed unique phosphorylation sites in autophagy-related proteins such as ULK2, RB1CC1, ATG16L1, and ATG9, suggesting that altered phosphorylation patterns contribute to impaired autophagic flux in ASD. SH-SY5Y cells with *SHANK3* gene deletion showed elevated LC3-II and p62 levels, indicating autophagosome accumulation and autophagy initiation, while the reduced level of the lysosomal activity marker LAMP1 suggested impaired autophagosome-lysosome fusion. The study highlights the involvement of reactive nitrogen species and nitric oxide (NO) on autophagy disruption. Importantly, inhibition of neuronal NO synthase (nNOS) by 7-NI normalized autophagy markers levels in the SH-SY5Y cells and primary cultured neurons. We have previously shown that nNOS inhibition improved synaptic and behavioral phenotypes in *Shank3*^{Δ4–22} and *Cntnap2*^{−/−} mouse models. Our multi-omics study reveals differential expression and phosphorylation of autophagy-related proteins in ASD but further investigation is needed to prove the full involvement of autophagy in ASD. Our study underscores the need for further examination into the functional consequences of the identified phosphorylation sites, which may offer potential novel therapeutic autophagy-related targets for ASD treatment.

Autism spectrum disorder (ASD) comprises a wide range of complex neurodevelopmental disorders that share the core neurobehavioral deficits manifested by abnormalities in social interactions and communication, restricted interests, repetitive behaviors, and intellectual disability¹. ASD is one of the most prevalent neurodevelopmental disorders. According to the Centers for Disease Control and Prevention (CDC), it affected 1 in 36 children in the United States in 2023, and its prevalence keeps rising every year². This disorder imposes a significant financial burden on the healthcare system, with costs projected to reach around 461 billion dollars by 2025³. ASD is over 90% inheritable^{4,5} but can also be caused by de novo gene variations⁶. The male-to-female ratio in ASD is considered to be 4:1. However, since the diagnostic criteria are mainly based on autistic males, it has been suggested that with effective female diagnosis, the ratio could reach up to 2:1^{7,8}.

In the last decade, many ASD-associated genes have been discovered, and many of these genes encode synaptic proteins. Some of them have been used to generate genetically engineered ASD mouse models. Two major genes associated with ASD are SH3 and multiple ankyrin repeat domains 3 (*SHANK3*), and the contactin-associated protein-like 2 gene (*CNTNAP2*).

Shank3 is a postsynaptic scaffold protein of excitatory synapses that connect neurotransmitter receptors, ion channels, and other membrane proteins with signaling proteins and the actin cytoskeleton. Through

¹Institute for Drug Research, School of Pharmacy, Faculty of Medicine, The Hebrew University of Jerusalem, Jerusalem, Israel. ²Rosamund Stone Zander Translational Neuroscience Center, Boston Children's Hospital, Boston, MA, USA. ³Department of Neurology, Boston Children's Hospital, Harvard Medical School, Boston, MA, USA. ✉email: Haitham.amal@mail.huji.ac.il

these protein interactions, Shank proteins construct signaling platforms that facilitate G-protein-mediated signaling and manage calcium homeostasis in dendritic spines⁹. They also play a role in synapse formation and dendritic spine maturation¹⁰. *SHANK3* mutations account for 1–2% of individuals with ASD¹¹. Among other neurological disorders carrying mutations or variations of *SHANK3* are schizophrenia¹², Alzheimer's disease¹³, and Phelan-McDermid syndrome¹⁴. *Cntnap2* is a presynaptic protein belonging to the neuroligin superfamily of transmembrane proteins. It plays a crucial role in synapse formation, synaptic transmission, the balance of excitatory and inhibitory post-synaptic currents (E/I balance), and neural development^{15,16}. Mutations of this gene are associated with multiple neurodevelopmental disorders, including schizophrenia¹⁷, intellectual disability¹⁸, attention deficit hyperactivity disorder¹⁹, and specific language impairment²⁰. In addition, *CNTNAP2* was one of the first genes discovered to be associated with an increased risk of ASD²¹.

While the exact causes of ASD are not fully understood, studying the shared molecular consequences followed by *Shank3* and *Cntnap2* mutations in the brain might bring about a better understanding of the underlying shared mechanisms of ASD. To this end, in this study, we employed a multi-omics approach aimed at better understanding the molecular networks and pathways of the proteins and their modifications involved in ASD pathology.

Global proteomics is designed to analyze the complete set of proteins expressed in a particular tissue sample at a given time, thus providing a broad overview of protein changes. Phosphoproteomics focuses on the identification and quantification of phosphorylated proteins. Phosphorylation is a common posttranslational modification (PTM) in which phosphate groups are added to specific amino acid residues, typically serine, threonine, or tyrosine. Phosphorylation plays a crucial role in protein activity regulation, signal transduction, and various cellular processes. Changes in phosphorylation patterns can manifest important events in cell signaling in health and disease²².

Nitric oxide (NO) is an essential regulator of protein function^{23,24} and is involved in various cellular processes in the brain in health and disease^{24–36}. NO was found to be elevated at early stages of neurodegeneration in Alzheimer's disease³⁷, and recently, our group has reported a dramatic increase in NO levels in ASD mouse models^{23,25,26,30,38–40,41}.

Utilizing a multi-omics approach that includes global- and phosphoproteomics linked to NO is particularly valuable in unraveling the complex biology of autism. By merging these methodologies, we can decipher the intricate interplay of protein alterations, PTMs, and signaling cascades in autism, paving the way for a more holistic and profound understanding of the disorder's molecular basis.

It has been shown that alterations in autophagy are present in various neurodevelopmental and neurodegenerative disorders^{42,43}. The term “autophagy” is derived from the Greek meaning “self-eating.” It is a crucial cellular process involving the degradation and recycling of various components such as damaged organelles, proteins, and cellular structures⁴⁴. This process is highly evolutionarily conserved in eukaryotes, playing a critical role in maintaining cellular health and homeostasis of cells in the body, mainly during cellular stress⁴⁵ and apoptosis^{46,47}. Autophagy holds significant importance in the brain, especially in neurons, which are post-mitotic cells that cannot be replaced⁴³. It maintains neuronal homeostasis by facilitating the degradation of misfolded proteins, eliminating damaged organelles, and regulating processes such as apoptosis and inflammation^{48,49}. However, if autophagy becomes impaired in neurons, it can lead to detrimental consequences, including the accumulation of ubiquitinated proteins, mitochondrial dysfunction, damage to axons and neural terminals, disruptions in synaptic neurotransmission, and ultimately, neurodegeneration^{24,50–52}. Autophagy is tightly regulated by a complex network of genes and signaling pathways. Dysregulation of autophagy has been implicated in various neurodevelopmental and neurodegenerative disorders^{24,42,43,53}, including Alzheimer's, Parkinson's, and Huntington's diseases, neuronal excitotoxicity, and cerebral ischemia^{42,48,54}. Autophagy is a multi-step process beginning with the formation of a double-membrane structure called a phagophore. During the elongation phase, the phagophore expands, capturing cellular components targeted for degradation and forming an autophagosome. At this point, degradation has not yet occurred⁵⁵. The autophagosome then fuses with a lysosome. Once fusion occurs, the degradation phase starts, and the lysosomal enzymes degrade the engulfed materials, leading to the nutrient release and recycling of cellular components into the cytoplasm^{56,57}.

The role of autophagy in ASD is of particular interest. Some studies suggest that autophagy overactivation is linked to ASD, while others indicate a reduced activity of autophagy in autism. For example, Dana et al. investigated the *Cc2d1a*^{+/-} ASD mouse model and revealed increased autophagy in females and decreased autophagy in males compared to the control group⁵⁸. The open-field test indicated that mostly female *Cc2d1a*^{+/-} mice exhibited aggressive and hyperactive behaviors⁵⁸. This study emphasizes the importance of studying both sexes in research related to neurodevelopmental disorders such as ASD. In another study using a rat model of ASD induced by valproate (VPA), the ASD mice exhibited a lack of autophagosomes and lower expression of the autophagy marker, LC3-II, compared to the control⁵⁹. In this study, the researchers inhibited the mechanistic target of rapamycin (mTOR) protein, a crucial inhibitory regulator of autophagy, and observed a significant increase in autophagosome formation in the treated VPA mice. These findings underscore the potential role of mTOR-mediated autophagy dysfunction in the pathogenesis of ASD^{59,60}. Furthermore, an additional study employing the *Tsc2*^{+/-} ASD mouse model, characterized by constitutively overactive mTOR, revealed autophagy deficiency. Another transgenic ASD mouse model in this study, based on *ATG7* knockout (KO), displayed similar phenotypes⁶¹. *ATG7* is a protein essential for autophagy, downstream of mTOR, suggesting that autophagy deficiency may be responsible for the underlying deficits caused by mTOR hyperactivation⁶¹.

Considering these data and beyond, autophagy emerges as a focal point of interest in ASD pathology^{24,59,61}. It is essential to explore the connection between autophagy and ASD to understand the complex molecular mechanisms that underlie this neurodevelopmental condition. Consequently, our objective was to ascertain if and how autophagy is modified in different ASD mouse models, specifically in *Shank3*^{Δ4-22} and *Cntnap2*^{-/-}.

mice. We aimed to identify how these modifications manifest in the multi- omics and examined if these changes are consistent across the models.

Materials and methods

Primary antibodies, LC-3A/B (#4108), LAMP1(#3243), and β -actin (#3700), secondary antibodies, HRP-conjugated anti-rabbit (7076S), and HRP conjugated anti-mouse (7074S), Anti-Rabbit Alexa fluor 594 (#8889), Anti-mouse Alexa Fluor 488 (#4408), ProLong gold Antifade with DAPI (#8961) and protease phosphatase inhibitor cocktail (#5872) were purchased from Cell Signaling Technology (Danvers, MA, USA). p62 primary antibody (ab109012) was purchased from Abcam (Cambridge, UK). Other general chemicals were purchased from Sigma Aldrich (St. Louis, MO, USA) and Bio-Rad Laboratories (Haifa, Israel).

Mouse models

All animal experiments were carried out in compliance with the guidelines set by the Institutional Animal Care and Use Committee at the Hebrew University of Jerusalem and the Association for Assessment and Accreditation of Laboratory Animal Care International. The study was conducted in accordance with the ARRIVE guidelines.

This study was approved by Committee at the Hebrew University of Jerusalem. The approved ethical number for this study, by Committee at the Hebrew University of Jerusalem, is IACUC-MD-20-16049-3.

Shank3^{Δ4-22} (Strain #:03 2169), *Cntnap2*^{-/-} (Strain #:01 7482), and C57BL/6J (Strain #:000664) were purchased from the Jackson Laboratory (Farmington, CT, USA). The *Shank3*^{Δ4-22} mice strain is generated by deleting exons 4–22 of the gene encoding the Shank3 protein. Hetero-male *Shank3*^{Δ4-22} mice were mated with hetero-female *Shank3*^{Δ4-22} mice. Three genotypes were obtained: WT, hetero, and homo *Shank3*^{Δ4-22} mice. WT littermates and homo *Shank3*^{Δ4-22} mice were used in the experiments. For the *Cntnap2*^{-/-} model, homozygous mating pairs were used. C57BL/6J mice were used as controls for *Cntnap2*^{-/-}. Male *Shank3*^{Δ4-22}, *Cntnap2*^{-/-}, and their respective littermates were used in this study. The mice were anesthetized with ketamine 200mg/kg body weight intramuscular and xylazine 10mg/kg body weight intraperitoneal. The mice were euthanized by cervical dislocation under the influence of sedation or anesthesia.

SH-SY5Y cell cultures and drug treatment

Human neuroblastoma SH-SY5Y cells were obtained from the American Type Culture Collection (ATCC) and maintained in Dulbecco's modified Eagle's medium (DMEM) and Ham's F-12 (1:1) supplemented with 10% fetal bovine serum, 2 mM L-glutamine, and 100 U/ml penicillin-G/100 mg/ml streptomycin in the humidified atmosphere (37 °C, 5% CO₂). Cells were plated onto 25 cm² and 75 cm² at a density of 7.0 × 10⁵ and 2.1 × 10⁶ cells/cm² respectively for Western blotting (WB). The SH-SY5Y cells were treated with 100 μM 7-nitroindazole (7-NI) for 24h⁶². This concentration was confirmed in our previous study. Mutant *Shank3* KO SH-SY5Y cells were generated in our lab using CRISPR-Cas9 technology as described in our last study²⁶.

Primary cultured neurons

Primary cortical neurons were isolated from fetal mouse brains on embryonic days 16–17 and grown as described previously²³. Dissections were performed in HBSS media and plated on poly-D-lysine-coated plates using Neural Basal media supplemented with L-glutamine, B27, and Penicillin/Streptomycin. Experiments were performed on DIV 14.

Confocal microscopy

Cells were fixed with 4% PFA for 20 min, washed 3 times with PBS, and blocked (3% BSA, 0.3% Triton X- 100 in PBS) for 30 min, all at room temperature. Cells were incubated with anti-p62 and anti-MAP2 (1:1000), antibodies overnight at 4 °C, followed by incubation with AlexaFluor-488 or -594-conjugated secondary antibodies (1:1000) for 1h. Then mounted with the nucleus fluorescent probe DAPI. Finally, the cells were observed (100×) under a Nikon confocal microscope.

Cell lysate preparation and Western blots (WB)

Cells were lysed in ice-cold RIPA buffer containing 50 mM Tris-HCl, 1% Nonidet P-40, 0.25% sodium deoxycholate, 150 mM NaCl, protease and phosphatase inhibitor cocktails, pH 7.4. After sonication, the lysates were centrifuged at 17,000 g for 30 min at 4 °C, and the supernatant was collected. The protein concentrations were determined with the BCA protein assay (Thermo Scientific, USA). Proteins were resolved by SDS-PAGE, transferred to a PVDF membrane, and probed with the appropriate primary antibodies and respective HRP-conjugated secondary antibodies. The blots were then visualized using an enhanced chemiluminescence (ECL) system⁶³. The full blots are shown in Supplementary Figs. 4, 5 and 6.

Mass spectrometry (MS) sample preparation

Tissue was lysed with 5% SDS in 50 mM Tris-HCl. Lysates were incubated at 96 °C for 5 min, followed by six cycles of 30 s of sonication (Bioruptor Pico, Diagenode, USA). Protein concentration was measured using the BCA protein assay. A total of 110 μg of protein was reduced with 5 mM dithiothreitol and alkylated with 10 mM iodoacetamide in the dark. Each sample was loaded onto S-Trap mini columns (Protifi, USA) according to the manufacturer's instructions. In brief, after loading, samples were washed with 90:10% methanol/50 mM ammonium bicarbonate. Samples were then digested with trypsin (1:50 trypsin/protein) for 1.5 h at 47 °C. The digested peptides were eluted using 50 mM ammonium bicarbonate; trypsin was added to this fraction and incubated overnight at 37 °C. Two more elutions were made with 0.2% formic acid and 0.2% formic acid in 50% acetonitrile. The three elutions were pooled together and vacuum-centrifuged to dry. Samples were kept

at -80°C until analysis⁶⁴. The samples were analyzed in The Mantoux Bioinformatics institute of the Nancy and Stephen Grand Israel National Center for Personalized Medicine, Weizmann Institute of Science.

Immobilized metal affinity chromatography

After digestion, 100 μg of each sample (*Shank3*^{Δ4–22}, *Shank3* WT, *Cntnap2*^{−/−}, and C57BL/6J) was subjected to phosphopeptide enrichment with AssayMAP Fe(III)-NTA cartridges (Agilent Technologies) using a Bravo robot (Agilent Technologies) according to the manufacturer's instructions. In brief, cartridges were primed and equilibrated with 250 μL of buffer A containing 99.9% acetonitrile (ACN) and 0.1% trifluoroacetic acid (TFA), and 100 μL of buffer B containing 80% ACN, 19.9% H_2O , and 0.1% TFA. The samples were loaded with 100 μL of buffer B at the rate of 5 $\mu\text{L}/\text{min}$. Then, the phosphopeptides were eluted with 50 μL of buffer C containing 99% H_2O and 1% NH_3 at 5 $\mu\text{L}/\text{min}$. 10 μL of formic acid was added to each sample for acidification. Prior to liquid chromatography (LC)–MS analysis, all samples were dried down⁶⁴.

Liquid chromatography-mass spectrometry

The ultra-LC–MS procedure was performed exactly as described previously⁶⁴.

Data processing

Raw data were processed with MaxQuant v1.6.6.0 or v2.0.1.0 software^{65,66}. The data were searched with the Andromeda search engine against the UniProt murine proteome database appended with common lab protein contaminants and the following modifications: Carbamidomethylation of C as a fixed modification, oxidation of M and protein N-terminal acetylation as variable ones. Phosphorylation of S, T, and Y were also added for the phospho-site analysis. The rest of the parameters remained at default except for the following: minimal peptide length was set to 6, Label and Label-Free Quantification (LFQ) minimal ratio count was set to 1, a match between runs and Intensity-Based Absolute Quantitation calculation was enabled, and the protein quantification was done based on unique peptides only. The LFQ intensities were extracted and used for further calculations using Perseus v1.6.2.3 software⁶⁷. Decoy hits and proteins identified based on a modified peptide only were filtered out. The data were further filtered to include only proteins with at least 2 or 3 valid values in at least one of the groups. Protein expression imputation was performed with a random low-range normal distribution. A Student's t-test, after logarithmic transformation, was used to identify significant differences across the biological replica. Fold changes (FC) were calculated based on the ratio of geometric means of the compared groups. Phospho analysis was carried out using the phospho-sites table generated by MaxQuant software. The data were filtered as in the global proteomics analysis. The intensities were normalized by subtracting the median. Missing values were imputed by a low constant. Statistical analysis was done the same as for the protein expression.

Bioinformatics and statistics

For the global proteomics data analysis, proteins with significant P-value (< 0.05) and an FC greater than 1.3 or smaller than 0.76 were considered as differentially expressed proteins (DEPs). Since in the phosphoproteomics data, many sites were detected only in some of the samples, we used two methods to analyze it. First, we assigned sites that were not identified in the sample with a constant value (with an integer smaller than the minimal identified intensity). Then, we calculated FC and performed a t-test to obtain P-values. In the second method, we defined unique phosphorylation sites (UPSs), as sites in which phosphorylation was identified in some of the KO samples but not in any of the WT samples, and *vice-versa*.

Gene ontology (GO) enrichment analysis for biological processes (BP), molecular functions (MF), and cellular components (CC) was performed using STRING v11.5 software⁶⁸. The Benjamini–Hochberg correction⁶⁹ was used to generate FDR, and terms with FDR values below 0.05 were accepted. Cytoscape software was used to visualize the protein functional interaction network⁷⁰. The interaction score was set to 0.7. The ClueGo plugin of Cytoscape⁷¹ was used to perform GO terms grouping (Fig. 2C).

The graphs and data analyses on the MS data were generated using Python v3.10, along with the Pandas, NumPy, and Plotly packages. Autophagy animation was created using BioRender.com. Additionally, the Phosphosite database was used to identify the role of specific phosphorylation sites⁷². SFARI database⁷³ was also employed to extract autism risk genes. Genes with a score of 1–3 were considered as autism risk genes.

The WB and confocal microscopy data are presented as the mean \pm SEM. A one-way ANOVA test, followed by the Tukey's multiple comparison post hoc test was used. Bar graphs and statistical analysis were performed using Prism v9.3 software (GraphPad Software, San Diego, CA). Differences were considered statistically significant where $P < 0.05$.

Results

Global proteomic analysis

Initially, we mapped the cortical global proteome of the *Shank3*^{Δ4–22}, *Cntnap2*^{−/−} mice (*Shank3* and *Cntnap2* mice) and their wild-type mice (WT1 and WT2, respectively), and calculated each protein's FC and P-value. Then, a volcano plot was used to visualize the quantitative differences in the protein levels in the mutant cortex compared to the WT (Fig. 1A and B). In the cortex of *Shank3* mice, our analysis showed 55 significantly altered proteins. 13 out of 55 proteins were less abundant in the *Shank3* mutant (Supp. Table 1), and 42 were more abundant compared to the corresponding proteins in WT1 mice (Supp. Table 2). GO enrichment analysis revealed significant enrichment for 37 CC terms, many of which were synapse-related (Fig. 1C).

In the *Cntnap2* cortex, 41 DEPs were detected. Among them, 21 DEPs were downregulated (Fig. 1B and Supp. Table 3) and 20 were upregulated (Fig. 1B and Supp. Table 4). However, the GO enrichment analysis did not reveal any signaling pathways for *Cntnap2* DEPs. None of the DEPs were common to both *Shank3* and *Cntnap2* mouse models.

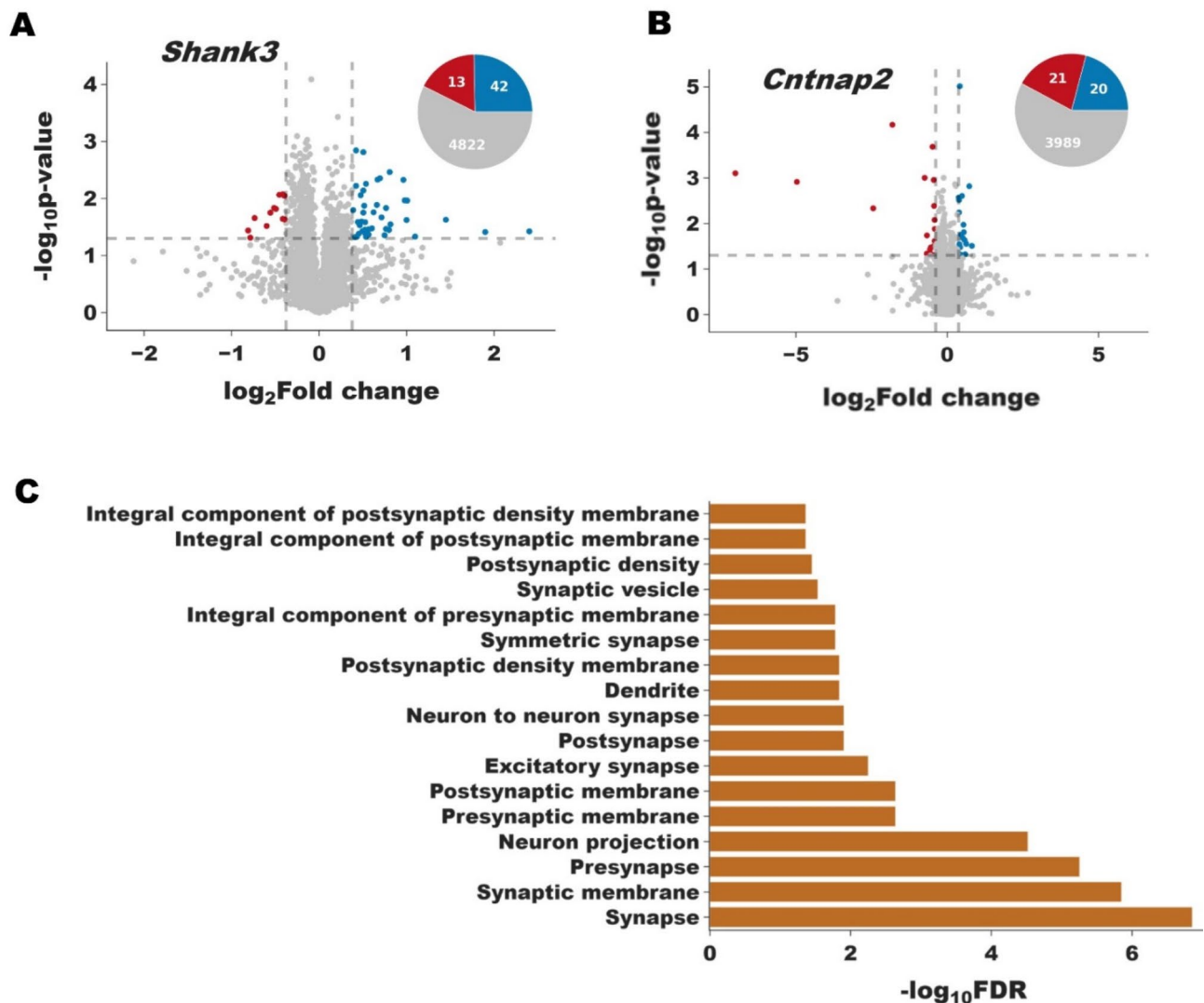


Fig. 1. Global differential expression analysis of *Shank3* mouse cortex proteins reveals changes in synaptic components. (A) Volcano plot of *Shank3* cortex proteins. Proteins with t-test p-value (un-corrected) smaller than 0.05 and fold-change greater than 1.3 or smaller than 0.76 were considered as differentially expressed proteins. Blue dots – upregulated proteins, red dots – downregulated proteins. Gray dots – insignificantly changed. Pie chart of the count of upregulated (blue), downregulated (red) out of the total number of protein detected (gray) proteins. (B) Volcano plot and pie chart of *Cntnap2* cortex proteins (p-values and FC were set as mentioned in A). (C) Gene ontology (GO) cellular component enriched terms of the DEP (both over- and under-expressed) from the *Shank3* cortex global samples. *Cntnap2* samples were not enriched for any term.

Phosphoproteomic analysis shared common enriched proteins related to synaptic transmission and synaptic plasticity in ASD mouse models

To capture the significant phosphorylation changes, UPS analysis was performed. 758 UPSs from 518 different proteins were identified in *Shank3* KO mice. 903 UPSs from 492 proteins were found in their WT counterparts. In *Cntnap2* KO mice, 190 UPSs from 148 different proteins were identified. 304 UPSs from 238 different proteins were identified in their respective WT mice. The intersection of the proteins exhibiting UPSs in the *Shank3* and *Cntnap2* models with SFARI ASD risk genes revealed a convergence of 26 proteins (hyper-geometric test $P < 0.001$) (Fig. 2A, Supp. List 1). 12 out of the 26 proteins formed cohesive protein functional interaction network (Fig. 2B). GO enrichment analysis of BP, MF, and CC on these proteins revealed that majority of the enriched terms are synaptic plasticity and synaptic transmission related terms (Fig. 2C) that are known to be altered in ASD^{74,75}.

UPSs showed enrichment of autophagy-related proteins in ASD mouse models

Next, we performed GO enrichment analysis on all the proteins containing UPSs. For both ASD mouse models, many of the enriched terms were related to synapse, synaptic plasticity, dendritic spine, neurogenesis, and brain

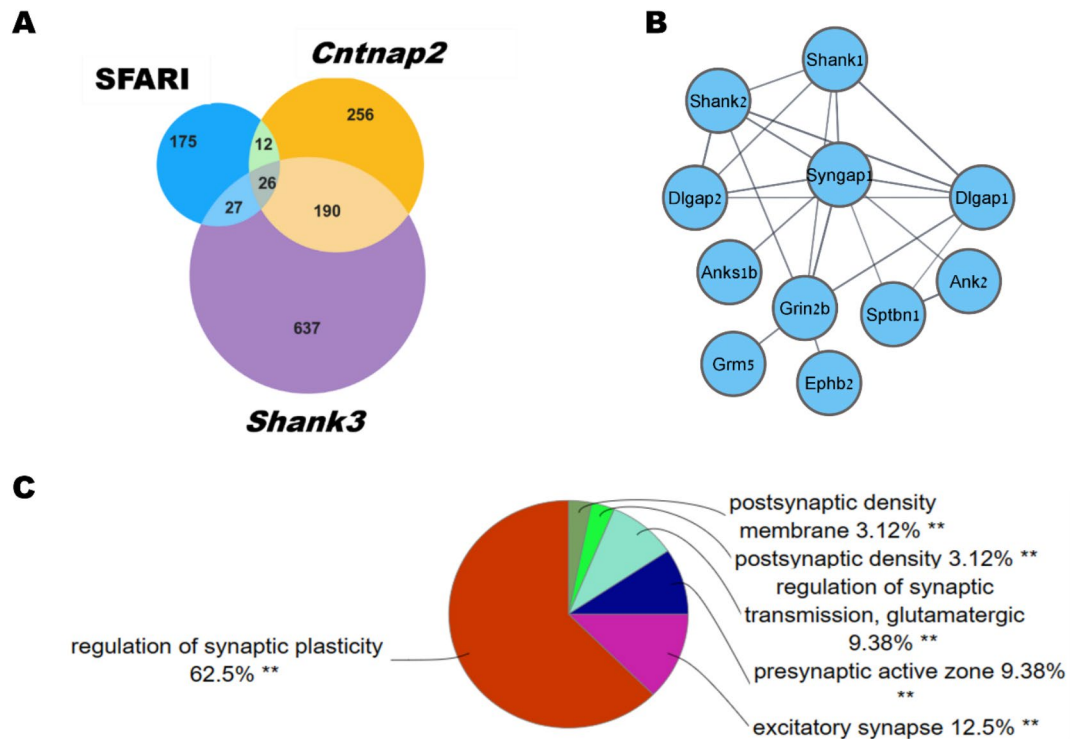


Fig. 2. Significant enrichment of ASD risk proteins in *Shank3* and *Cntnap2* mouse cortex UPSs containing proteins. **(A)** Venn diagram of the intersection of ASD-associated proteins from the SFARI database and proteins containing uniquely phosphorylated sites (UPSs) in *Shank3* and *Cntnap2* mice. Hypergeometric test $P < 0.0001$. **(B)** Protein functional interaction network of 12 out of the 26 SFARI proteins with UPSs shared among both *Shank3* and *Cntnap2* mice. **(C)** Pie chart of the enriched groups of GO terms from the 26 shared SFARI protein containing UPSs. Each slice represents % terms per group. The terms are grouped based on their ontology hierarchy. Created by ClueGO. ** $P < 0.001$.

development (Fig. 3A, B). Interestingly, significant enrichment of multiple terms related to autophagy was found for both models (Fig. 3A, B).

25 UPSs in autophagy-related proteins were found in *Shank3* mice. All of them were unique to the KO cortex. 17 UPSs in autophagy-related proteins were found in *Cntnap2* mice (unique to either KO or WT), with an overlap of 5 protein sites between the two models (sites were considered identical if their distance was no more than 3 amino acids, due to the MS specificity). The shared UPSs were: ATG16L1 at Ser254, PLEKHM2 at Ser423, SNX30 at Ser37, ATG9a at Ser15 for *Shank3* and Ser16 for *Cntnap2*, and CLTC at Ser70 for *Shank3* and Ser 67 for *Cntnap2*.

Differential phosphorylation of the core autophagy proteins in ASD mouse models

The autophagy proteins to which the UPSs belong encompass various steps within the autophagic process, including some that serve as core components. Unc-51-like autophagy activating kinase 2 (ULK2), which participates in the autophagy initiation stage as a member of the ULK complex^{76,77}, was uniquely phosphorylated at ser772 in the *Shank3* KO mice (Fig. 4A). RB1CC1, also known as FIP200, an additional member of the ULK complex, was significantly over-phosphorylated at Ser646 in *Shank3* mice compared to control ($P = 0.0076$, $FC = 1.54$; Fig. 4A), while its global protein levels were not changed. ATG9a, a protein participating in the phagophore nucleation stage and a downstream target of the ULK complex, was uniquely phosphorylated in both ASD models – in *Shank3* mice at Ser15 (Fig. 4A), and in *Cntnap2* at Ser16 (Fig. 4B). ATG16L1, a protein that directly interacts with RB1CC1 and participates in autophagosome formation, showed UPS at Thr254 in both *Shank3* and *Cntnap2* KO mice (Fig. 4A, B). The ATG16L1 protein interacts with WD repeat domain phosphoinositide-interacting protein 2 (WIPI2) (Fig. 4C), which had a UPS at Ser360 in *Cntnap2* mice. ATG7, a protein that plays a major role in autophagosome formation and LC3-I lipidation was found to be uniquely phosphorylated at Ser291 in *Shank3* mice (Fig. 4A). SQSTM, also known as p62, an autophagosome cargo protein and a recognized marker of autophagy^{78–80}, with central UPS containing proteins mentioned in Fig. 4C. Additional UPSs in autophagy proteins are shown in Supplementary Figs. 1–3.

Alterations in autophagic makers in ASD mouse models

Due to the limited information available in the literature regarding the specific role of individual phosphorylation sites, and to validate our findings concerning the direction of autophagy modulation, we reanalyzed our global

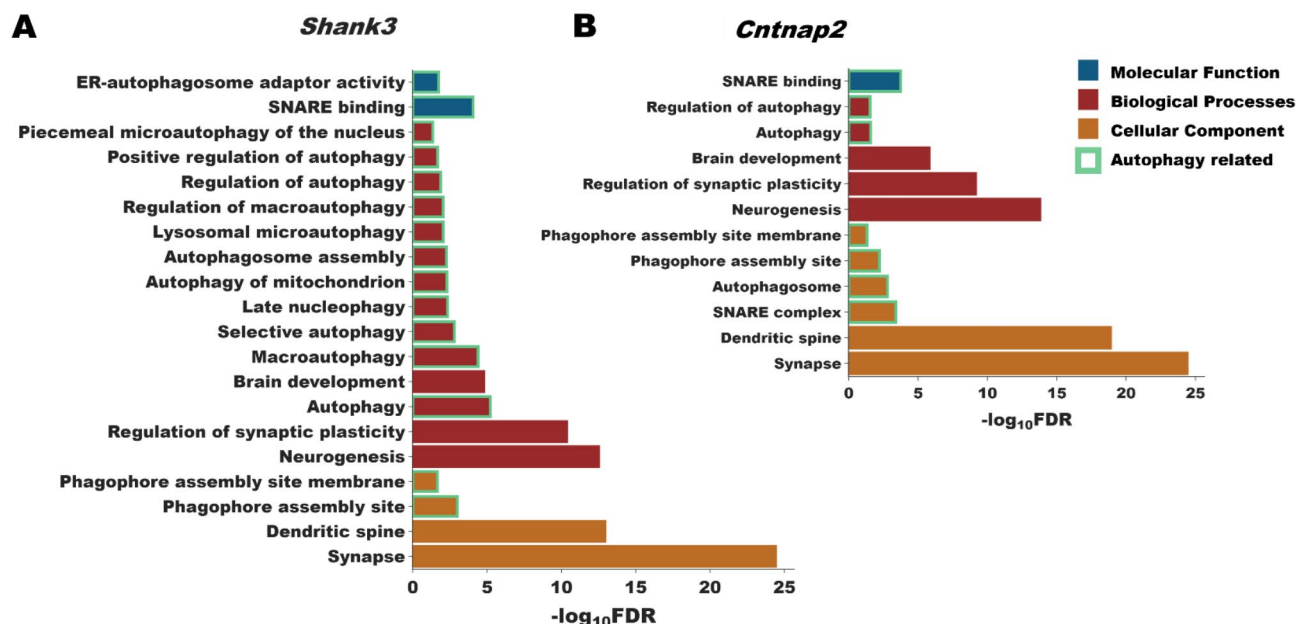


Fig. 3. Proteins containing UPSs show enrichment of autophagy terms. GO enrichment analysis of biological processes (BP), molecular function (MF), and cellular components (CC) for the cortical proteins with UPSs (A) for *Shank3* mice (only unique phosphorylated sites for the *Shank3* KO were analyzed), (B) for *Cntnap2* and WT2 mice (UPSs for *Cntnap2* and WT2 were analyzed together).

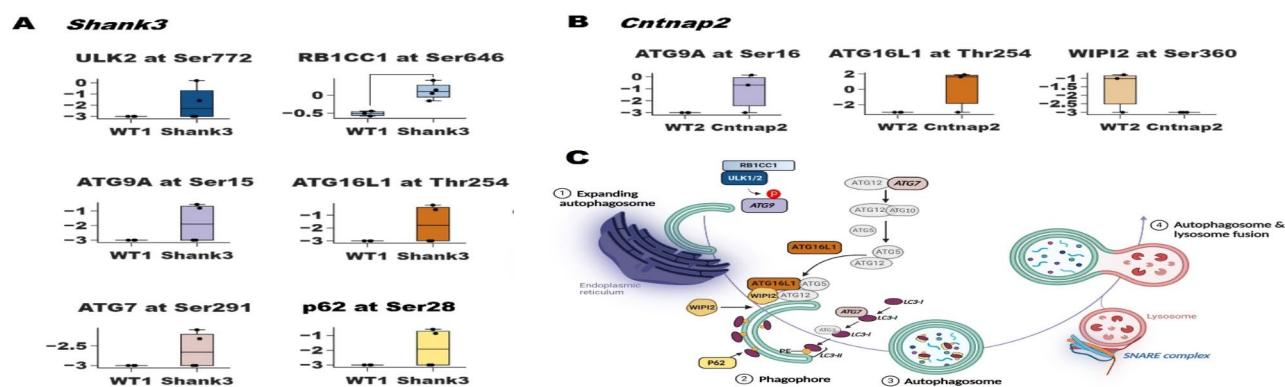


Fig. 4. Phosphorylation changes in core autophagy proteins in the mouse cortex. (A) Phosphorylated sites in *Shank3* mice. All the sites were phosphorylated only in the *Shank3* KO mice besides RB1CC1 at Ser646, which was phosphorylated in both *Shank3* and WT1 mice. However, this protein was significantly over-phosphorylated in *Shank3* KO ($P = 0.007$, $FC = 1.54$). Statistical analysis was not performed on the UPSs of the proteins since they were not identified (represented in the graph as the value -3). (B) UPSs in *Cntnap2* mice. ATG9A at Ser16 and ATG16L1 at Thr254 are UPS of *Cntnap2* KO, while WIPI2 at Ser360 is UPS of WT2. ATG16L1 and ATG9A are UPSs in the KO of both *Shank3* and *Cntnap2* models. (C) The molecular mechanism of autophagy, with central UPS containing proteins mentioned. Participating proteins are color-coded respectively to A and B. Created with BioRender.com.

proteomics dataset, focusing on autophagosomal marker proteins p62, and MAP1LC3. We found that the MAP1LC3A was significantly upregulated in *Cntnap2* ($FC = 1.31$, $P = 0.003$; Fig. 5A), whereas in *Shank3* mice, this protein was also overexpressed but did not reach a significance level ($FC = 1.25$, $P = 0.062$; Fig. 5B). No changes in the expression levels of p62 were detected in the global proteomics dataset for either model.

7-NI prevented imbalanced autophagy in the *Shank3* KO cells

To check the effect of RNS on autophagy, we tested the levels of different autophagic proteins in WT SH-SY5Y cells, *Shank3* KO SH-SY5Y cells, and *Shank3* KO SH-SY5Y cells treated with 7-NI (*Shank3* + 7-NI). 7-NI was shown to reverse ASD-like behaviors and synaptic deficits in the *Shank3* and *Cntnap2* mouse models²³. We tested the protein levels of p62, and LC3-II as these proteins are involved in autophagy initiation and

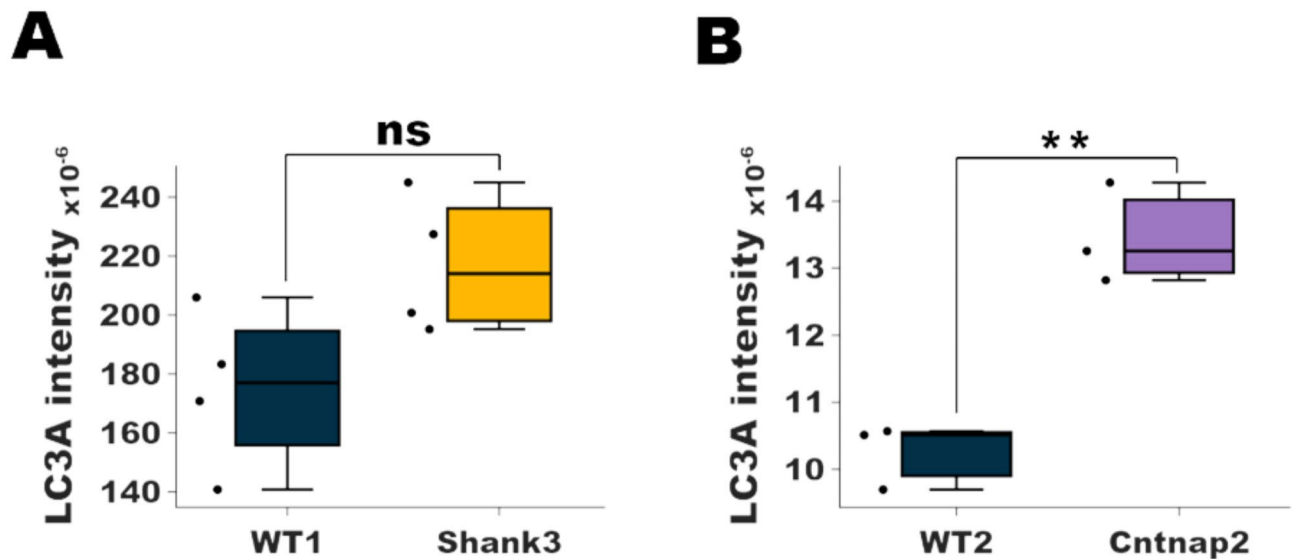


Fig. 5. Alterations in autophagy marker proteins (A) MAP1LC3A over-expressed (though not significantly) in the cortex of *Shank3* KO (t-test $P = 0.062$). (B) MAP1LC3A is significantly over-expressed in the cortex of *Cntnap2* mice (t-test $P = 0.004$).

autophagosome formation. The levels of p62, and LC3-II appeared to be elevated in *Shank3* KO SH-SY5Y cells as compared to their WT counterparts (Fig. 6A–C). We have also tested the levels of LAMP1 protein, which helps in autolysosome formation. We have found decreased levels of LAMP1 in *Shank3* KO cells as compared to WT showing decreased autolysosome formation (Fig. 6D). Overall, these results suggest imbalanced autophagy in the KO cells. Treatment of *Shank3* KO cells with 7-NI (100 μ M) for 24 h rescued autophagy protein levels to match the control. We found decreased levels of LC3-II and p62 whereas the levels of LAMP1 in *Shank3* KO cells treated with 7-NI were increased compared to the vehicle treated *Shank3* KO cells. Further, we also measured the fluorescence intensity of p62 in WT and *Shank3* KO primary cortical neurons. We found an increased fluorescence intensity of p62 in the *Shank3* KO compared to WT (Fig. 6E, F). Treatment of *Shank3* KO with 7-NI rescued p62 intensity compared to *Shank3* KO neurons treated with vehicle. Further, to confirm imbalanced autophagy, we measured autophagic flux. We have validated the Chloroquine dose in WT cortical neurons to test the autophagic flux (Supplementary Fig. 6)⁸¹. Further, we assessed autophagic flux in *Shank3* KO primary cultured neurons by treating them with Chloroquine (20 μ M) for 4h (Fig. 6G–I). We have found an increase in the level of LC3-II and p62 in the presence of chloroquine compared to WT-cultured neurons. We have found no significant changes in *Shank3* KO neurons treated with CQ compared to *Shank3* KO neurons treated with vehicle, which shows inhibition of autophagic flux in *Shank3* KO cells.

Discussion

Our multi-omics study delves into the molecular mechanisms of ASD with a focus on *Shank3* ^{$\Delta 4-22$} and *Cntnap2* ^{$-/-$} mouse models. Through global- and phospho- proteomics analyses, we aimed to unravel the shared molecular changes contributing to ASD pathogenesis, with a particular emphasis on autophagy.

The global proteomics analysis revealed a small number of DEPs in the cortex of *Shank3* and *Cntnap2* mice. For example, in the *Shank3* model, overexpression of solute carrier family 6 member 3 (SLC6A3), the protein encoded by the corresponding ASD risk gene, was observed. This protein is a dopamine transporter that regulates dopamine levels in the synaptic cleft⁸². In the *Cntnap2* model, two ASD-associated DEPs were found, tuberous sclerosis complex 2 (TSC2) and glutamate ionotropic receptor delta type subunit 1 (GRID1). Both proteins were downregulated. TSC2 is a tumor suppressor protein and the master negative regulator of mTOR complex 1 (mTORC1)⁸³. Its downregulation leads to the overactivation of mTORC1, followed by autophagy inhibition^{60,84}, and perhaps, could be involved in the observed alterations in the autophagy signal transduction cascades. The second ASD risk gene is *GRID1* which encodes a subunit of glutamate receptor channels. These channels mediate most of the fast excitatory synaptic transmission in the central nervous system and play key roles in synaptic plasticity⁸⁵.

GO enrichment analysis highlighted multiple synapse-related cellular component terms in the *Shank3* mouse model, emphasizing the importance of synaptic phenotype in ASD pathology. In the *Cntnap2* mouse model, DEPs were not enriched for GO terms (probably due to the small number of DEPs). Despite the relatively small number of DEPs found in both models, these changes appear to contribute to the synaptic alterations known to be associated with ASD, which promote the behavioral deficits that appeared in these models in our previous studies^{8,23,25,40}.

Meanwhile, our phosphoproteomics analysis identified multiple unique phosphorylation sites (UPSs) in both models. The UPSs were enriched for ASD-related proteins. Among them, 26 proteins were uniquely phosphorylated in both models and 12 of them appeared to form a functional interaction network, indicating

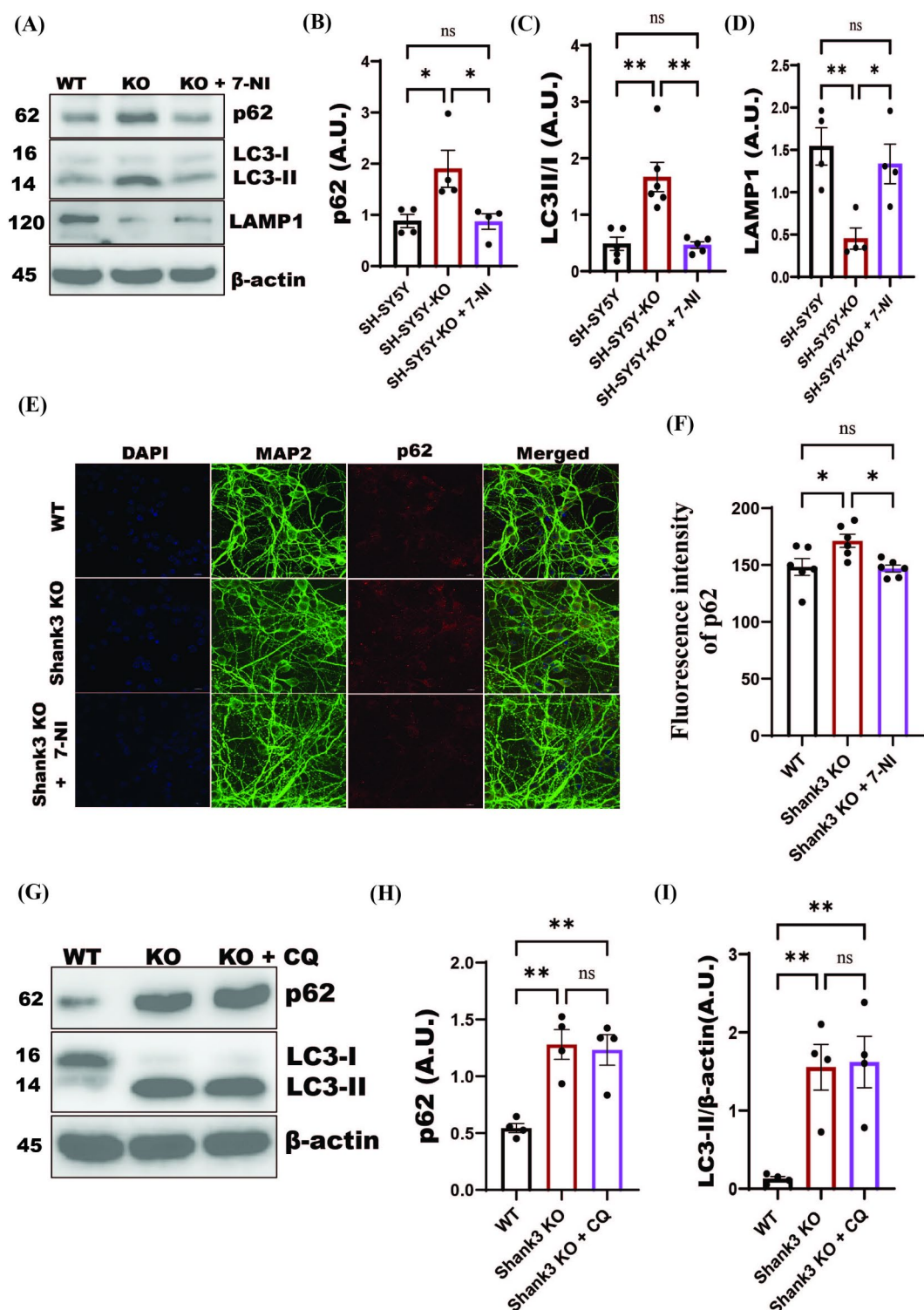


Fig. 6. 7-NI reversed the levels of autophagy-related proteins: (A) Representative Western blot images of p62, LC3-II, and LAMP1 in the WT, *Shank3* KO, and *Shank3* KO + 7-NI SH-SY5Y cells. β -actin was used as a loading control. (B–D) Statistical analysis of the relative abundance of p62 (n = 4 in each group), LC3-II (n = 5 in each group), and LAMP1 (n = 4 in each group). (E) Representative confocal images of MAP2 (green), p62 (red), and DAPI (blue) in the WT, *Shank3* KO, and *Shank3* KO + 7-NI primary cortical neurons. (F) Statistical analysis of fluorescence intensity of p62 in the WT, *Shank3* KO, and *Shank3* KO + 7-NI (n = 6, in each group) cells. The image was captured at 100 \times magnification, and the scale bar = 20 μ m (G) Representative Western blot images of p62 and LC3-II in the WT, *Shank3* KO, and *Shank3* KO + CQ in primary cultured cortical neuron. β -actin was used as a loading control. (H, I) Statistical analysis of the relative abundance of p62 (n = 4) and LC3-II (n = 4) in each group. A one-way ANOVA test with Tukey's multiple comparison tests in all groups. *p < 0.05, **p < 0.01, ns = non-significant.

a convergence of *Shank3* and *Cntnap2* ASD pathogenic mechanisms, and pointing toward common alterations in the regulation of synaptic plasticity and transmission. We observed several key synaptic proteins, including Dlgap1, Dlgap2, Shank1, Shank2, Shank3, Syn1, Rims1, Pclo, Syngap1, Stxbp1, Grin2b, Camk2a, Ephb2, and Ank2. These proteins play crucial roles in synaptic structure, neurotransmission, and plasticity. For instance, the Shank family proteins (Shank1, Shank2, and Shank3) act as scaffolding molecules at the postsynaptic density, stabilizing synaptic architecture and influencing signaling pathways⁸⁶. Syn1 regulates neurotransmitter release⁸⁷, whereas Stxbp1 is critical for synaptic vesicle fusion⁸⁸. Grin2b, a subunit of NMDA receptors, modulates synaptic strength and plasticity^{89,90}, while Camk2a participates in long-term potentiation (LTP) through phosphorylation events⁹¹. It is noteworthy that many proteins involved in synaptic plasticity are regulated by phosphorylation⁹². Therefore, alterations in this PTM are likely to be linked to synaptic dysfunction and may play a critical role in ASD pathology. Furthermore, the multiple changes in phosphorylation levels observed in the ASD mouse models, without the corresponding alterations in the global protein expression levels, suggest that the changes in cell signaling might be crucial for ASD pathology.

The UPSs found in both models were significantly enriched in autophagy-related proteins encompassing various steps of the autophagic processes, including some of the core components of these processes. Among these proteins, ULK2, which contained UPS in the *Shank3* mice, stands out as it is a key member of the ULK complex, also known as the autophagy activating complex which includes ULK1/2, ATG13, RB1CC1, and ATG101⁷⁶. ULK is known to be directly phosphorylated by mTORC1 and AMP-activated protein kinase (AMPK). mTOR is a central cell-growth regulator integrating growth factors and nutrient signals⁹³. As previously noted, TSC2 acts as a negative regulator of mTORC1. Downregulation of TSC2 leads to mTORC1 activation, which subsequently inhibits autophagy via suppression of the ULK complex⁹⁴. Although in the literature ULK1 is mentioned in the context of mTOR-dependent autophagy, ULK2 can replace ULK1 in the ULK complex. These two proteins share significant structural similarity, contain similar kinase domains, and are part of the same kinase family⁹⁵. They were shown to exhibit functional redundancy in some aspects of autophagy regulation, but independent roles have also been reported⁹⁵.

In the initial stages of autophagosome biogenesis, the formation and subsequent activation of the ULK kinase complex play a crucial role in ensuring the proper nucleation of the phagophore and its expansion into a functional autophagosome^{24,43}. Another important member of the ULK complex that showed altered phosphorylation is RB1CC1, which directly interacts with ULK as part of the ULK complex⁹⁶. Although this protein did not have a UPS, it was significantly over-phosphorylated in the cortex of *Shank3* KO mice at Ser646. RB1CC1 directly interacts with ATG16L1, a protein containing UPS at the same location in both ASD models. The interaction between RB1CC1 and ATG16L1 is specifically required for ULK complex-dependent autophagy⁹⁷. ATG16L1 plays a role in phagophore membrane expansion and autophagosome formation. This protein interacts with WIPI2 and recruits the ATG12-ATG5-ATG16L1 complex to the phagophore⁹⁸. In both *Shank3* and *Cntnap2* KO mice, ATG16L1 is phosphorylated at the same site, Thr254 (Fig. 4A, B). Furthermore, the WIPI2 protein was found to have UPS at Ser360 in *Cntnap2* WT mice (Fig. 4B).

The ULK complex phosphorylates and regulates numerous core ATG proteins. A notable example of a core ATG protein undergoing ULK-dependent phospho-regulation is ATG9, which is also a protein containing UPS in both ASD models, at Ser15 for *Shank3* KO (Fig. 4A) and Ser16 for *Cntnap2* KO (Fig. 4B). ATG9 is an exclusive conserved multi-spanning membrane protein within the core ATG machinery. It is localized in cytoplasmic vesicles and tubules and participates in the phagophore nucleation^{99,100}. In response to starvation, ULK phosphorylates ATG9A at Ser14 and thus leads to the repositioning of ATG9A vesicles from the trans-Golgi network to endosomes followed by the autophagy initiation¹⁰¹.

Another important ATG is ATG7 which plays a pivotal role in autophagosome formation, functioning as an E1-like activating enzyme crucial for the initial phases of autophagy¹⁰². Its functions include the activation of ATG12 for subsequent conjugation with ATG5 to assemble the construction of the ATG12-ATG5-ATG16L1 complex. We found the unique ATG7 phosphorylation at Ser291 in *Shank3* mice (Fig. 4A). No data on the role of this site are currently available in the literature, and its function needs further investigation.

The ATG12-ATG5-ATG16L1 complex is also known to facilitate the lipidation of light chain 3 (LC3)-I with phosphatidylethanolamine, leading to the formation of LC3-II¹⁰². During the autophagosome formation process, LC3-I, the freely diffusible form of LC3, is converted to LC3-II, the membrane-anchored, lipidated form of LC3⁵³. Thus, an increase in the levels of LC3-II is indicative of autophagosome formation and is used as an autophagy marker. The protein that directs protein aggregates and cytoplasmic bodies marked for degradation into the autophagosome is p62. This important molecule serves as an autophagosome cargo protein, possessing multiple domains that enable cargo sequestration. It is noteworthy that among its functional motifs, there is the PB1 domain, which functions as a protein-protein interaction module, the LC3-interacting region that mediates the interaction of p62 with LC3-II, and the ubiquitin-associated domain that interacts with ubiquitinated proteins marked for proteasomal degradation^{103,104}. In this process, p62 is degraded, and its levels are decreased when autophagy is induced. Thus, p62 levels can be an indicator of autophagic flux¹⁰⁵. We found p62 to have UPS at Ser28 (localized in the PB1 domain¹⁰⁶) in *Shank3* mice (Fig. 4A).

A protein that appeared to have UPSs in both models is Pleckstrin homology and RUN domain containing M2 (PLEKHM2). PLEKHM2 is responsible for lysosome localization. Recently, it has been suggested that this protein is involved in the functional development of neurons as a regulator of autophagic flux¹⁰⁷. PLEKHM2 was phosphorylated at Ser423 in *Shank3* and *Cntnap2* KO mice (Supp. Figs. 1, 2). The observed phosphorylation changes in PLEKHM2 may be associated with the reduced lysosomal activity in *Shank3* KO cells, as evidenced by the decreased expression levels of LAMP1 compared to the control.

The protein sorting nexin-30 (SNX30), involved in autophagosome assembly¹⁰⁸, was found to be uniquely phosphorylated at Ser37 in *Shank3* KO mice, while in the *Cntnap2* model, it was uniquely phosphorylated at the

same site in the WT control mice (Supp. Figs. 1, 3), suggesting a potential point of divergence between the two models that should be further investigated.

The observed alterations in the phosphorylation status of key autophagy-related proteins suggest a dysregulation of the intricate regulatory mechanisms of autophagy in ASD. This observation led us to investigate autophagy markers in SH-SY5Y cells with *SHANK3* deletion. Western blot analysis revealed elevated levels of the autophagy markers LC3-II, suggesting autophagosome accumulation¹⁰⁹. Conversely, the downstream lysosomal activity marker—LAMP1, was downregulated, and p62 upregulated, implying reduced lysosomal activity and impaired autophagosome-lysosome fusion. This increase in p62 can be the result of S-nitrosylation of p62, as after S-nitrosylation of p62 make it does not undergo ubiquitination and also inhibits autophagic flux^{110,111}. Additionally, we found no significant change in the level of p62 and LC3-II in *Shank3* KO neurons in the presence of Chloroquine as compared to *Shank3* KO with no treatment, showing inhibition of autophagic flux. Together, these findings point to a dysregulation of the autophagy process. We later inhibited nNOS with 7-NI and we found decreased level of p62 and LC3-II. Overall, these findings suggest RNS mediated autophagy dysregulation in these cells¹¹⁰.

Apparently, the expression and PTMs of autophagy-related proteins may vary in different ASD models. Thus, Dana et al.⁵⁸ found that LC3 levels were elevated in female and decreased in male mice of the *Cc2d1a*^{+/-} model of ASD. In another study, Lieberman et al.¹¹² found decreased LC3B-II, and increased levels of p62 in the VPA mouse model of ASD, indicating reduced activity of autophagy in the process of development in these mice. Importantly, these changes were observed at P28 but not P10, showing that the activity of autophagy processes depends on the stage of development. Our results and the work of others clearly indicate dysregulation of autophagy in ASD. In addition, the functions of many phosphorylation sites identified in this work remain unknown and require further investigation to uncover their involvement in autophagy.

Dysregulation of autophagy in the *Shank3* model of ASD

Abnormal activation of the mTOR signaling pathway in ASD has been identified in numerous studies¹¹³. Previous work by our group demonstrated enrichment of the mTOR pathway in S-nitrosylated proteins within the brain of the *Shank3* ASD mouse model⁶⁰. Overactivation of mTORC1 inhibits autophagy through phosphorylation and inactivation of the autophagy-activating ULK complex^{24,113}. Our data revealed that both ULK2 and RB1CC1, the key components of the ULK complex, contain UPSs in the *Shank3* KO mouse model. Under normal conditions, this complex induces autophagy by activating the class III PI3K protein complex, with Beclin1 as a key component. In ASD, elevated mTOR levels typically inhibit mTOR-dependent autophagy. A study by Linda et al.¹¹⁴ on the neurodevelopmental disorder Koolen-de Vries Syndrome (KdVS), reported similar expression patterns, including elevated levels of p62 and LC3-II, alongside increased mTOR activity and reduced LAMP1 expression. They suggested that these findings may indicate a compensatory mechanism for autophagy initiation, potentially driven by the increased oxidative stress observed. Furthermore, they propose that the balance between mTOR-dependent autophagy and reactive oxygen species (ROS)-dependent autophagy is disrupted. Increased mTOR activity inhibits the ULK complex and reduces lysosomal activity, thus impairing autophagy. At the same time, elevated oxidative stress promotes autophagy. However, since mTOR also impairs lysosomal function¹¹⁵, autophagosome-lysosome fusion is compromised, leading to the accumulation of autophagosomes, as indicated by elevated levels of the autophagosome marker LC3-II. Consequently, the autophagy process is dysregulated and ineffective. This disruption prevents the proper sequestration of cellular waste, potentially contributing to synaptic dysfunction and the associated behavioral phenotype.

Our data support this proposed mechanism and suggest that the increase in reactive nitrogen species (RNS), particularly nitric oxide (NO), which we found to be elevated in the *Shank3* and *Cntnap2* models²³, enhances ROS/RNS-dependent autophagy initiation on the background of impaired lysosomal activity. The latter may prevent autophagosome fusion with lysosomes, leading to the autophagy breakdown in these ASD models (Fig. 7). Indeed, the addition of 7-NI, a neuronal NO synthase inhibitor, to *SHANK3* KO cells restored the expression levels of p62, LC3-II, and LAMP1, indicating normalization of autophagy. Additionally, previous research from our group demonstrated that 7-NI treatment in *Shank3* and *Cntnap2* KO models rescued both synaptic and behavioral phenotypes^{23,25}. Here, we propose that the functional autophagy restoration contributes to the observed beneficial effects of the nNOS inhibition.

Previous studies have established the involvement of autophagy in the regulation of synaptic plasticity and transmission¹¹⁶. Our comprehensive analysis, integrating global and phospho- supports this concept and offers valuable insights into autophagy's involvement in the molecular mechanisms underlying ASD. The global proteomics analysis identified a limited number, yet important differentially expressed proteins, which appear to significantly impact synaptic dysfunction, a known hallmark of ASD pathology. Importantly, the differential expression of proteins such as SLC6A3 in the *Shank3* model and TSC2 and GRID1 in the *Cntnap2* model underscores the involvement of the key pathways in ASD, including dopamine regulation, mTORC1 signaling, and synaptic transmission.

The phosphoproteomics analysis further revealed significant changes in phosphorylation status, particularly in proteins related to autophagy and synaptic plasticity, indicating that these PTMs may play a crucial role in ASD pathogenesis. The identification of the unique phosphorylation sites in core autophagy-related proteins, such as ULK2, ATG16L1, and ATG9, suggests that the dysregulation of autophagy in ASD may be mediated through altered phosphorylation patterns, potentially leading to impaired autophagic flux.

Our findings align with the above-mentioned mechanism proposed by Linda et al.¹¹⁴, which describes the interplay between mTOR-dependent and ROS-dependent autophagy. We extend this hypothesis to the *Shank3* ASD model, particularly emphasizing the role of RNS, and nitrosative and oxidative stress in driving autophagy dysregulation.

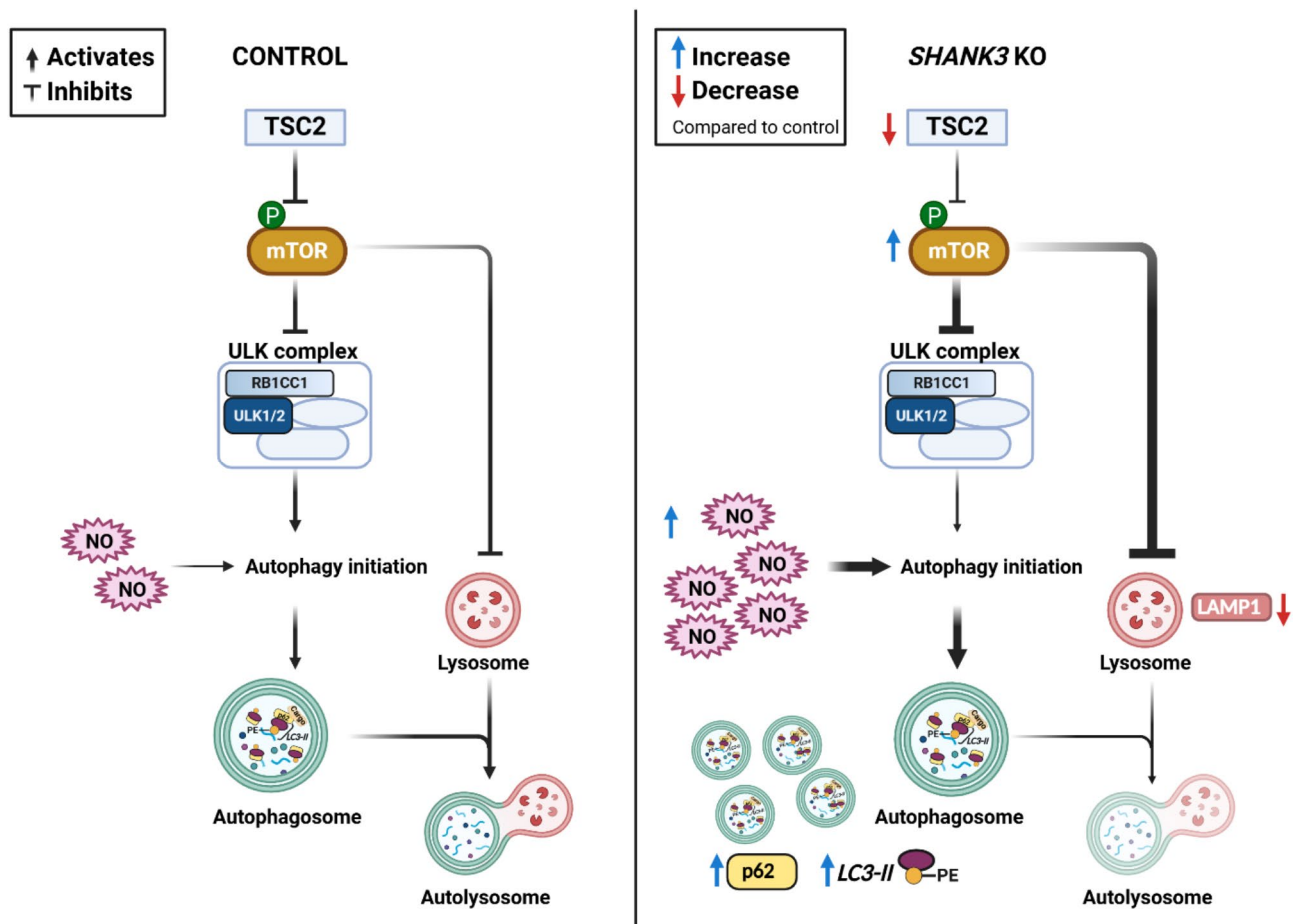


Fig. 7. Dysregulation of autophagy in *Shank3* model of ASD. In the *Shank3* model of ASD, downregulation of TSC2 results in the overactivation of mTOR, which subsequently inhibits the ULK complex and mTOR-dependent autophagy. Additionally, mTOR overactivation reduces lysosomal activity. Concurrently, an increase in RNS levels and nitrosative stress in *Shank3* KO mice induces ROS/RNS-dependent autophagy and autophagy initiation. This disruption in the balance between the two autophagy pathways impairs autophagosome-lysosome fusion due to reduced lysosomal activity, leading to autophagosome accumulation and ineffective autophagy.

Moreover, the restoration of autophagy markers upon inhibition of nNOS in *SHANK3* KO cells provides a potential therapeutic avenue for normalizing autophagy and reversing the ASD-like phenotypes. Our study not only supports the emerging view of autophagy dysregulation in ASD but also underscores the need for further investigation into the functional consequences of the identified phosphorylation sites, which may offer potential novel therapeutic autophagy-related targets for ASD treatment. While our findings present intriguing insights into the potential molecular mechanisms underlying ASD pathology, it is imperative to acknowledge that the results of this study need to be subjected to further validation. In conclusion, this multi-omics study significantly enhances our understanding of ASD pathology by unraveling the molecular intricacies associated with *Shank3* and *Cntnap2* mouse models.

Data availability

Data is provided within the manuscript or supplementary information files.

Received: 25 October 2024; Accepted: 24 March 2025

Published online: 29 March 2025

References

1. Sauer, A. K., Stanton, J. E., Hans, S. & Grubner, A. M. Autism spectrum disorders: etiology and pathology. In *Autism Spectrum Disorders* (ed Grubner, A. M.) (Exon Publications, 2021).
2. Li, Q. et al. Prevalence of autism spectrum disorder among children and adolescents in the United States from 2019 to 2020. *JAMA Pediatr.* **176**, 943–945 (2022).
3. Leigh, J. P. & Du, J. Brief report: forecasting the economic burden of autism in 2015 and 2025 in the United States. *J. Autism Dev. Disord.* **45**, 4135–4139 (2015).
4. Shastri, B. S. Molecular genetics of autism spectrum disorders. *J. Hum. Genet.* **48**, 495–501 (2003).

5. Sandin, S. et al. The heritability of autism spectrum disorder. *JAMA* **318**, 1182–1184 (2017).
6. Rylaarsdam, L. & Gomez-Gamboa, A. Genetic causes and modifiers of autism spectrum disorder. *Front. Cell Neurosci.* **13**, 385 (2019).
7. Posserud, M. B., Skretting Solberg, B., Engeland, A., Haavik, J. & Klungsoyr, K. Male to female ratios in autism spectrum disorders by age, intellectual disability and attention-deficit/hyperactivity disorder. *Acta Psychiatr. Scand.* **144**, 635–646 (2021).
8. Tripathi, M. K. et al. Mutations associated with autism lead to similar synaptic and behavioral alterations in both sexes of male and female mouse brain. *Sci. Rep.* **14**, 10 (2024).
9. Kreienkamp, H. J. Scaffolding proteins at the postsynaptic density: Shank as the architectural framework. In *Handb Exp Pharmacol* 365–380 (2008).
10. MacGillavry, H. D., Kerr, J. M., Kassner, J., Frost, N. A. & Blanpied, T. A. Shank-cortactin interactions control actin dynamics to maintain flexibility of neuronal spines and synapses. *Eur. J. Neurosci.* **43**, 179–193 (2016).
11. Moessner, R. et al. Contribution of SHANK3 mutations to autism spectrum disorder. *Am. J. Hum. Genet.* **81**, 1289–1297 (2007).
12. Zhang, J., Sun, X. Y. & Zhang, L. Y. MicroRNA-7/Shank3 axis involved in schizophrenia pathogenesis. *J. Clin. Neurosci.* **22**, 1254–1257 (2015).
13. Zhao, Y., Jaber, V. R., LeBeauf, A., Sharfman, N. M. & Lukiw, W. J. microRNA-34a (miRNA-34a) mediated down-regulation of the post-synaptic cytoskeletal element SHANK3 in sporadic Alzheimer's disease (AD). *Front. Neurol.* **10**, 28 (2019).
14. Zwanenburg, R. J., Ruiter, S. A., van den Heuvel, E. R., Flapper, B. C. & Van Ravenswaaij-Arts, C. M. Developmental phenotype in Phelan-McDermid (22q13.3 deletion) syndrome: A systematic and prospective study in 34 children. *J. Neurodev. Disord.* **8**, 16 (2016).
15. St George-Hyslop, F., Kivisild, T. & Livesey, F. J. The role of contactin-associated protein-like 2 in neurodevelopmental disease and human cerebral cortex evolution. *Front. Mol. Neurosci.* **15**, 1017144 (2022).
16. Lu, P. et al. A novel CNTNAP2 mutation results in abnormal neuronal E/I balance. *Front. Neurol.* **12**, 712773 (2021).
17. Friedman, J. I. et al. CNTNAP2 gene dosage variation is associated with schizophrenia and epilepsy. *Mol. Psychiatry* **13**, 261–266 (2008).
18. Zweier, C. Severe intellectual disability associated with recessive defects in CNTNAP2 and NRXN1. *Mol. Syndromol.* **2**, 181–185 (2012).
19. Elia, J. et al. Rare structural variants found in attention-deficit hyperactivity disorder are preferentially associated with neurodevelopmental genes. *Mol. Psychiatry* **15**, 637–646 (2010).
20. Whitehouse, A. J., Bishop, D. V., Ang, Q. W., Pennell, C. E. & Fisher, S. E. CNTNAP2 variants affect early language development in the general population. *Genes Brain Behav.* **10**, 451–456 (2011).
21. Li, D. et al. Common variants of the autism-associated CNTNAP2 gene contribute to the modulatory effect of social function mediated by temporal cortex. *Behav. Brain Res.* **409**, 113319 (2021).
22. Ardito, F., Giuliani, M., Perrone, D., Troiano, G. & Lo Muzio, L. The crucial role of protein phosphorylation in cell signaling and its use as targeted therapy. *Int. J. Mol. Med.* **40**, 271–280 (2017).
23. Tripathi, M. K. et al. The NO answer for autism spectrum disorder. *Adv. Sci.* (2023).
24. Khaliulin, I., Hamoudi, W. & Amal, H. The multifaceted role of mitochondria in autism spectrum disorder. *Mol. Psychiatry* (2024).
25. Abdel-Haq, M. et al. Effects of extended-release 7-nitroindazole gel formulation treatment on the behavior of Shank3 mouse model of autism. *Nitric Oxide* (2023).
26. Bazbaz, W. et al. The role of thioredoxin system in Shank3 Mouse model of autism. *J. Mol. Neurosci.* **74**, 90 (2024).
27. Kruglyakov, D. et al. Nitric oxide synthase inhibition prevents cell proliferation in glioblastoma. *J. Mol. Neurosci.* 1–9 (2023).
28. Yang, H. et al. Mechanistic insight into female predominance in Alzheimer's disease based on aberrant protein S-nitrosylation of C3. *Sci. Adv.* **8**, eade0764 (2022).
29. Tripathi, M. K., Kartawy, M., Ginzburg, S. & Amal, H. Arsenic alters nitric oxide signaling similar to autism spectrum disorder and Alzheimer's disease-associated mutations. *Transl. Psychiatry* **12**, 127 (2022).
30. Kartawy, M., Khaliulin, I. & Amal, H. Systems biology reveals S-nitrosylation-dependent regulation of mitochondrial functions in mice with Shank3 mutation associated with autism spectrum disorder. *Brain Sci.* **11** (2021).
31. Hamoudi, W. et al. Regional differences in S-nitrosylation in the cortex, striatum, and hippocampus of juvenile male mice. *J. Mol. Neurosci.* 1–10 (2021).
32. Kartawy, M., Khaliulin, I. & Amal, H. Systems biology reveals reprogramming of the S-nitroso-proteome in the cortical and striatal regions of mice during aging process. *Sci. Rep.* **10**, 1–11 (2020).
33. Khaliulin, I., Kartawy, M. & Amal, H. Sex differences in biological processes and nitrergic signaling in mouse brain. *Biomedicine* **8**, 124 (2020).
34. Amal, H. et al. Low doses of arsenic in a mouse model of human exposure and in neuronal culture lead to S-nitrosylation of synaptic proteins and apoptosis via nitric oxide. *Int. J. Mol. Sci.* **21**, 3948 (2020).
35. Amal, H. et al. S-nitrosylation of E3 ubiquitin-protein ligase RNF213 alters non-canonical Wnt/Ca²⁺ signaling in the P301S mouse model of tauopathy. *Transl. Psychiatry* **9**, 44 (2019).
36. Ojha, S. K. & Amal, H. Air pollution: An emerging risk factor for autism spectrum disorder. *Brain* **1**, 4 (2024).
37. Seneviratne, U. et al. S-nitrosation of proteins relevant to Alzheimer's disease during early stages of neurodegeneration. *Proc. Natl. Acad. Sci. U. S. A.* **113**, 4152–4157 (2016).
38. Tripathi, M. K., Kartawy, M. & Amal, H. The role of nitric oxide in brain disorders: Autism spectrum disorder and other psychiatric, neurological, and neurodegenerative disorders. *Redox Biol.* **34**, 101567 (2020).
39. Steinert, J. R. & Amal, H. The contribution of an imbalanced redox signalling to neurological and neurodegenerative conditions. *Free Radic. Biol. Med.* **194**, 71–83 (2023).
40. Hamoudi, W., Tripathi, M. K., Ojha, S. K. & Amal, H. A cross-talk between nitric oxide and the glutamatergic system in a Shank3 mouse model of autism. *Free Radic. Biol. Med.* **188**, 83–91 (2022).
41. Amal, H. et al. Shank3 mutation in a mouse model of autism leads to changes in the S-nitroso-proteome and affects key proteins involved in vesicle release and synaptic function. *Mol. Psychiatry* **25**, 1835–1848 (2020).
42. Deng, Z., Zhou, X., Lu, J. H. & Yue, Z. Autophagy deficiency in neurodevelopmental disorders. *Cell Biosci.* **11**, 214 (2021).
43. Rana, T. et al. Exploring the role of autophagy dysfunction in neurodegenerative disorders. *Mol. Neurobiol.* **58**, 4886–4905 (2021).
44. Yorimitsu, T. & Klionsky, D. J. Autophagy: Molecular machinery for self-eating. *Cell Death Differ.* **12**(Suppl 2), 1542–1552 (2005).
45. He, L. et al. Autophagy: The last defense against cellular nutritional stress. *Adv. Nutr.* **9**, 493–504 (2018).
46. Vijayakumar, K. & Cho, G. W. Autophagy: An evolutionarily conserved process in the maintenance of stem cells and aging. *Cell Biochem. Funct.* **37**, 452–458 (2019).
47. Doherty, J. & Baehrecke, E. H. Life, death and autophagy. *Nat. Cell Biol.* **20**, 1110–1117 (2018).
48. Li, Y., Qin, Z. H. & Sheng, R. The multiple roles of autophagy in neural function and diseases. *Neurosci. Bull.* (2023).
49. Cai, Z. et al. Chaperone-mediated autophagy: Roles in neuroprotection. *Neurosci. Bull.* **31**, 452–458 (2015).
50. Wang, Y., Song, M. & Song, F. Neuronal autophagy and axon degeneration. *Cell Mol. Life Sci.* **75**, 2389–2406 (2018).
51. Shen, D. N., Zhang, L. H., Wei, E. Q. & Yang, Y. Autophagy in synaptic development, function, and pathology. *Neurosci. Bull.* **31**, 416–426 (2015).
52. Kenney, D. L. & Benarroch, E. E. The autophagy-lysosomal pathway: General concepts and clinical implications. *Neurology* **85**, 634–645 (2015).

53. Dikic, I. & Elazar, Z. Mechanism and medical implications of mammalian autophagy. *Nat. Rev. Mol. Cell Biol.* **19**, 349–364 (2018).
54. Tripathi, M. K., Rajput, C., Mishra, S., Rasheed, M. S. U. & Singh, M. P. Malfunctioning of chaperone-mediated autophagy in Parkinson's disease: Feats, constraints, and flaws of modulators. *Neurotox. Res.* **35**, 260–270 (2019).
55. Mizushima, N. Autophagy: Process and function. *Genes Dev.* **21**, 2861–2873 (2007).
56. Glick, D., Barth, S. & Macleod, K. F. Autophagy: Cellular and molecular mechanisms. *J. Pathol.* **221**, 3–12 (2010).
57. Lin, Y. H., Huang, Y. C., Chen, L. H. & Chu, P. M. Autophagy in cancer stem/progenitor cells. *Cancer Chemother. Pharmacol.* **75**, 879–886 (2015).
58. Dana, H. et al. Disregulation of autophagy in the transgenerational Cc2d1a mouse model of autism. *Neuromol. Med.* **22**, 239–249 (2020).
59. Zhang, J., Zhang, J. X. & Zhang, Q. L. PI3K/AKT/mTOR-mediated autophagy in the development of autism spectrum disorder. *Brain Res. Bull.* **125**, 152–158 (2016).
60. Mencer, S. et al. Proteomics of autism and Alzheimer's mouse models reveal common alterations in mTOR signaling pathway. *Transl. Psychiatry* (2021).
61. Tang, G. et al. Loss of mTOR-dependent macroautophagy causes autistic-like synaptic pruning deficits. *Neuron* **83**, 1131–1143 (2014).
62. Fujibayashi, T. et al. Mitogen-activated protein kinases regulate expression of neuronal nitric oxide synthase and neurite outgrowth via non-classical retinoic acid receptor signaling in human neuroblastoma SH-SY5Y cells. **129**, 119–126 (2015).
63. Choi, Y. R. et al. Prion-like propagation of α -synuclein is regulated by the Fc γ RIIB-SHP-1/2 signaling pathway in neurons. **22**, 136–148 (2018).
64. Elinger, D., Gabashvili, A. & Levin, Y. Suspension trapping (S-Trap) is compatible with typical protein extraction buffers and detergents for bottom-up proteomics. *J. Proteome Res.* **18**, 1441–1445 (2019).
65. Cox, J. & Mann, M. MaxQuant enables high peptide identification rates, individualized p.p.b.-range mass accuracies and proteome-wide protein quantification. *Nat. Biotechnol.* **26**, 1367–1372 (2008).
66. Cox, J. et al. Accurate proteome-wide label-free quantification by delayed normalization and maximal peptide ratio extraction, termed MaxLFQ. *Mol. Cell Proteomics* **13**, 2513–2526 (2014).
67. Tyanova, S. et al. The Perseus computational platform for comprehensive analysis of (prote)omics data. *Nat. Methods* **13**, 731–740 (2016).
68. Szklarczyk, D. et al. STRING v10: Protein–protein interaction networks, integrated over the tree of life. *Nucleic Acids Res.* **43**, D447–D452 (2015).
69. Benjamini, Y. & Hochberg, Y. Controlling the false discovery rate: A practical and powerful approach to multiple testing. *J. R. Stat. Soc. Ser. B Stat. Methodol.* **57**, 289–300 (1995).
70. Shannon, P. et al. Cytoscape: A software environment for integrated models of biomolecular interaction networks. *Genome Res.* **13**, 2498–2504 (2003).
71. Bindea, G. et al. ClueGO: A Cytoscape plug-in to decipher functionally grouped gene ontology and pathway annotation networks. *Bioinformatics* **25**, 1091–1093 (2009).
72. Hornbeck, P. V., Chabra, I., Kornhauser, J. M., Skrzypek, E. & Zhang, B. PhosphoSite: A bioinformatics resource dedicated to physiological protein phosphorylation. *Proteomics* **4**, 1551–1561 (2004).
73. Banerjee-Basu, S. & Packer, A. SFARI Gene: An evolving database for the autism research community. *Dis. Model Mech.* **3**, 133–135 (2010).
74. Rhee, J., Park, K., Kim, K. C., Shin, C. Y. & Chung, C. Impaired hippocampal synaptic plasticity and enhanced excitatory transmission in a novel animal model of autism spectrum disorders with telomerase reverse transcriptase overexpression. *Mol. Cells* **41**, 486–494 (2018).
75. Giovedì, S., Corradi, A., Fassio, A. & Benfenati, F. Involvement of synaptic genes in the pathogenesis of autism spectrum disorders: The case of synapsins. *Front. Pediatr.* **2**, 94 (2014).
76. Zachari, M. & Ganley, I. G. The mammalian ULK1 complex and autophagy initiation. *Essays Biochem.* **61**, 585–596 (2017).
77. Alers, S., Löffler, A. S., Wesselborg, S. & Stork, B. Role of AMPK-mTOR-Ulk1/2 in the regulation of autophagy: cross talk, shortcuts, and feedbacks. *Mol. Cell Biol.* **32**, 2–11 (2012).
78. Collier, J. J., Suomi, F., Oláhová, M., McWilliams, T. G. & Taylor, R. W. Emerging roles of ATG7 in human health and disease. *EMBO Mol. Med.* **13**, e14824 (2021).
79. Mizushima, N. The ATG conjugation systems in autophagy. *Curr. Opin. Cell Biol.* **63**, 1–10 (2020).
80. Li, X., He, S. & Ma, B. Autophagy and autophagy-related proteins in cancer. *Mol. Cancer* **19**, 12 (2020).
81. Guo, S. et al. A rapid and high content assay that measures cyto-ID-stained autophagic compartments and estimates autophagy flux with potential clinical applications. *Autophagy* **11**, 560–572 (2015).
82. Reith, M. E. A. et al. The dopamine transporter gene SLC6A3: multidisease risks. *Mol. Psychiatry* **27**, 1031–1046 (2022).
83. Dunkerly-Eyring, B. L. et al. Single serine on TSC2 exerts biased control over mTORC1 activation mediated by ERK1/2 but not Akt. *Life Sci. Alliance* **5** (2022).
84. Chan, E. Y. mTORC1 phosphorylates the ULK1-mAtg13-FIP200 autophagy regulatory complex. *Sci. Signal.* **2**, pe51 (2009).
85. Hruska, M., Cain, R. E. & Dalva, M. B. Nanoscale rules governing the organization of glutamate receptors in spine synapses are subunit specific. *Nat. Commun.* **13**, 920 (2022).
86. Sheng, M. & Kim, E. The Shank family of scaffold proteins. *J. Cell Sci.* **113**, 1851–1856 (2000).
87. Hilfiker, S. et al. Synapsins as regulators of neurotransmitter release. *Philos. Trans. R. Soc. Lond. Ser. B Biol. Sci.* **354**, 269–279 (1999).
88. Melland, H., Arvell, E. H. & Gordon, S. L. Disorders of synaptic vesicle fusion machinery. *J. Neurochem.* **157**, 130–164 (2021).
89. Paoletti, P., Bellone, C. & Zhou, Q. NMDA receptor subunit diversity: Impact on receptor properties, synaptic plasticity and disease. *Nat. Rev. Neurosci.* **14**, 383–400 (2013).
90. Myers, S. J. et al. Distinct roles of GRIN2A and GRIN2B variants in neurological conditions. *F1000Research* **8**, 1940 (2019).
91. Lisman, J., Yasuda, R. & Raghavachari, S. Mechanisms of CaMKII action in long-term potentiation. *Nat. Rev. Neurosci.* **13**, 169–182 (2012).
92. Lee, H. K. Synaptic plasticity and phosphorylation. *Pharmacol. Ther.* **112**, 810–832 (2006).
93. Kim, J. & Guan, K.-L. mTOR as a central hub of nutrient signalling and cell growth. *Nat. Cell Biol.* **21**, 63–71 (2019).
94. Wong, P.-M., Puente, C., Ganley, I. G. & Jiang, X. The ULK1 complex: sensing nutrient signals for autophagy activation. *Autophagy* **9**, 124–137 (2013).
95. Demeter, A. et al. ULK1 and ULK2 are less redundant than previously thought: Computational analysis uncovers distinct regulation and functions of these autophagy induction proteins. *Sci. Rep.* **10**, 10940 (2020).
96. Li, L. et al. RB1CC1-enhanced autophagy facilitates PSCs activation and pancreatic fibrogenesis in chronic pancreatitis. *Cell Death Dis.* **9**, 952 (2018).
97. Gammoh, N., Florey, O., Overholtzer, M. & Jiang, X. Interaction between FIP200 and ATG16L1 distinguishes ULK1 complex-dependent and -independent autophagy. *Nat. Struct. Mol. Biol.* **20**, 144–149 (2013).
98. Wilson, M. I., Dooley, H. C. & Tooze, S. A. WIPI2b and Atg16L1: Setting the stage for autophagosome formation. *Biochem. Soc. Trans.* **42**, 1327–1334 (2014).
99. Licheva, M., Raman, B., Kraft, C. & Reggiori, F. Phosphoregulation of the autophagy machinery by kinases and phosphatases. *Autophagy* **18**, 104–123 (2022).

100. Deneubourg, C. et al. The spectrum of neurodevelopmental, neuromuscular and neurodegenerative disorders due to defective autophagy. *Autophagy* **18**, 496–517 (2022).
101. Zhou, C. et al. Regulation of mATG9 trafficking by Src- and ULK1-mediated phosphorylation in basal and starvation-induced autophagy. *Cell Res.* **27**, 184–201 (2017).
102. Liu, K. et al. MicroRNA-106a inhibits autophagy process and antimicrobial responses by targeting ULK1, ATG7, and ATG16L1 during mycobacterial infection. *Front. Immunol.* **11**, 610021 (2020).
103. Liu, W. J. et al. p62 links the autophagy pathway and the ubiquitin-proteasome system upon ubiquitinated protein degradation. *Cell Mol. Biol. Lett.* **21**, 29 (2016).
104. Lin, X. et al. Interaction domains of p62: a bridge between p62 and selective autophagy. *DNA Cell Biol.* **32**, 220–227 (2013).
105. Ichimura, Y. & Komatsu, M. Selective degradation of p62 by autophagy. *Semin. Immunopathol.* **32**, 431–436 (2010).
106. Gao, J. et al. Cytosolic PINK1 promotes the targeting of ubiquitinated proteins to the aggresome-autophagy pathway during proteasomal stress. *Autophagy* **12**, 632–647 (2016).
107. Ben-Zvi, H., Rabinski, T., Ofir, R., Cohen, S. & Vatine, G.D. PLEKHM2 loss of function impairs the activity of iPSC-derived neurons via regulation of autophagic flux. *Int. J. Mol. Sci.* **23** (2022).
108. Antón, Z. et al. A heterodimeric SNX4–SNX7 SNX-BAR autophagy complex coordinates ATG9A trafficking for efficient autophagosome assembly. *J. Cell Sci.* **133** (2020).
109. Tanida, I., Ueno, T. & Kominami, E. LC3 and autophagy. In *Autophagosome and Phagosome* 77–88 (2008).
110. Oh, C.-K. et al. S-Nitrosylation of p62 inhibits autophagic flux to promote α -synuclein secretion and spread in Parkinson's disease and Lewy body dementia. *J. Neurosci.* **42**, 3011–3024 (2022).
111. Kim, K.-R. et al. S-Nitrosylation of cathepsin B affects autophagic flux and accumulation of protein aggregates in neurodegenerative disorders. *Cell Death Differ.* **29**, 2137–2150 (2022).
112. Lieberman, O. J. et al. mTOR suppresses macroautophagy during striatal postnatal development and is hyperactive in mouse models of autism spectrum disorders. *Front. Cell. Neurosci.* **14**, 70 (2020).
113. Winden, K. D., Ebrahimi-Fakhari, D. & Sahin, M. Abnormal mTOR activation in autism. *Annu. Rev. Neurosci.* **41**, 1–23 (2018).
114. Linda, K. et al. Imbalanced autophagy causes synaptic deficits in a human model for neurodevelopmental disorders. *Autophagy* **18**, 423–442 (2022).
115. Carosi, J. M., Fourrier, C., Bensalem, J. & Sargeant, T. J. The mTOR–lysosome axis at the centre of ageing. *FEBS Open Bio* **12**, 739–757 (2022).
116. Liang, Y. emerging concepts and functions of autophagy as a regulator of synaptic components and plasticity. *Cells* **8** (2019).

Acknowledgements

We thank the Satell Family Foundation and the Neubauer Family Foundation for their support.

Author contributions

E.D.: Data analysis, figures generation and manuscript writing, S.O.: mice handling and biochemistry, M.K.: data analysis, I.K.: discussion and manuscript writing, H.A.: manuscript writing, discussion, and project supervision.

Funding

This work was funded by a US Department of Defense (DoD) grant, a DFG – German Research Foundation Grant, an Israeli Science Foundation (ISF) grant, an Eagles Autism Foundation grant, a National Institute of Psychobiology in Israel (NIPI) grant, and a Berettler Centre for Research in Molecular Pharmacology and Therapeutics Grant.

Declarations

Competing interests

Haitham Amal is a CSO of Point6 Bio and Neuro-NOS. No funds from both companies were received for this study. All other authors do not hold any competing interests.

Additional information

Supplementary Information The online version contains supplementary material available at <https://doi.org/10.1038/s41598-025-95860-8>.

Correspondence and requests for materials should be addressed to H.A.

Reprints and permissions information is available at www.nature.com/reprints.

Publisher's note Springer Nature remains neutral with regard to jurisdictional claims in published maps and institutional affiliations.

Open Access This article is licensed under a Creative Commons Attribution-NonCommercial-NoDerivatives 4.0 International License, which permits any non-commercial use, sharing, distribution and reproduction in any medium or format, as long as you give appropriate credit to the original author(s) and the source, provide a link to the Creative Commons licence, and indicate if you modified the licensed material. You do not have permission under this licence to share adapted material derived from this article or parts of it. The images or other third party material in this article are included in the article's Creative Commons licence, unless indicated otherwise in a credit line to the material. If material is not included in the article's Creative Commons licence and your intended use is not permitted by statutory regulation or exceeds the permitted use, you will need to obtain permission directly from the copyright holder. To view a copy of this licence, visit <http://creativecommons.org/licenses/by-nc-nd/4.0/>.

© The Author(s) 2025